Inorganic Chemistry

Article

pubs.acs.org/IC

In Solution Sensitization of Er(III) Luminescence by the 4-Tetrathiafulvalene-2,6-pyridinedicarboxylic Acid Dimethyl Antenna Ligand

Fabrice Pointillart,[†] Adrien Bourdolle,[‡] Thomas Cauchy,[§] Olivier Maury,*[,‡] Yann Le Gal,[†] Stéphane Golhen,[†] Olivier Cador,[†] and Lahcène Ouahab*[,†]

[†]Organométalliques et Matériaux Moléculaires, UMR 6226 CNRS-UR1 Sciences Chimiques de Rennes, Université de Rennes 1, 35042 Rennes Cedex, France

[‡]Laboratoire de Chimie, UMR 5182 CNRS-ENS Lyon-Université Lyon 1, 46 Allée d'Italie, 69364 Lyon Cedex 07, France

[§]Laboratoire MOLTECH-Anjou, Université d'Angers CNRS-UMR 6200, 2 Bd Lavoisier, 49045 Angers, France

Supporting Information

ABSTRACT: In the $[Er(hfac)_3(\mathbf{L})]_2$ complex (**1**) (**L** = 4-tetrathiafulvalene-2,6-pyridinecarboxylic acid dimethyl ester), the Er(III) ion is bonded to the tridentate coordination site. Electrochemical and photophysical measurements in solution reveal that the tetrathiafulvalene moiety is a versatile antenna for erbium luminescence sensitization at 6540 cm^{-1} upon excitation in the low-energy charge transfer transition (donor to acceptor charge transfer) at 16600 cm^{-1} assigned via time-dependent density functional theory calculations.

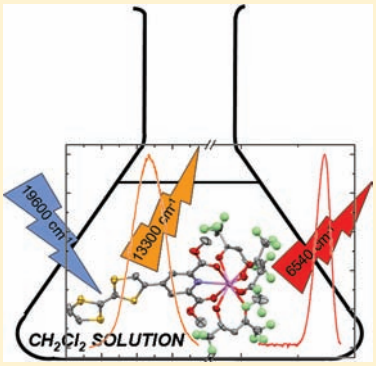

INTRODUCTION

The tetrathiafulvalene (TTF)-based molecular materials interest both physical and chemical communities aiming to establish an interplay or synergy between two or more properties.[1,2] Very recently, we showed that TTF derivatives can effectively sensitize the near-infrared (NIR) solid state luminescence of 4f elements as Yb(III) and Nd(III) ions, opening the way for luminescence.[3] The Yb(III) ion is a very unusual case of a lanthanide ion, as it has only one single excited state and its sensitization mechanism can involve (i) a classical transfer of energy from an antenna ligand, (ii) a photoinduced electron transfer via an Yb(II),[4] or (iii) a charge-separated state intermediate.[5] On the other hand, in the aforementioned Nd(III) complex, the presence of the f–f transitions complicates the determination of the sensitization mechanism.[3a] In these previous cases, TTF-based ligands led to the formation of complexes isolated only in the crystalline state, and their solution instability is a major drawback for the further preparation of materials. Therefore, it seemed to us it is now crucial to extend the scope of the TTF-based ligand to the solution and to the last NIR emitters, Er(III). To that end, we decided to start from a tridentate dipicolic acid ligand known to give more stable 1:1 complexes under its ester or amide forms[6] and to present functionalization opportunity at position 4 to optimize the photophysical properties.[7] We report here the design and preparation of new 4-tetrathiafulvalene-2,6-pyridinecarboxylic acid dimethyl ester (**L**) ligand and the related Er(III) complex of the general formula $[Er(hfac)_3(\mathbf{L})]_2$ (**1**) ($hfac^-$ = 1,1,1,5,5,5-hexafluoroacetylacetonate). The X-ray structure of the ligand and the related complex will be described. Finally, their photophysical properties were measured in solution and in the solid state and are discussed on the basis of time-dependent density functional theory (TD-DFT) calculation.

EXPERIMENTAL SECTION

Synthesis. *General Procedures and Materials.* Tributylstannyl-tetrathiafulvalene and 4-iodo-2,6-pyridinedicarboxylic acid dimethyl ester compounds were synthesized following reported methods.[8,9] All the other reagents were purchased from Aldrich Co. Ltd. and were used without further purification.

4-Tetrathiafulvalene-2,6-pyridinedicarboxylic Acid Dimethyl Ester (L). Tributylstannyl-tetrathiafulvalene (0.6 g, 1.22 mmol) was dissolved in 55 mL of distilled toluene, and then 4-iodo-2,6-pyridinedicarboxylic acid dimethyl ester (0.4 g, 1.25 mmol) followed by $Pd(PPh_3)_4$ (0.072 g, 0.06 mmol) was added under an argon atmosphere. The solution was stirred for 24 h under reflux. After this, the solvent was removed under vacuum and the residue dissolved in 175 mL of CH_2Cl_2 and an aqueous solution of NH_4F (1 M) (6.526 g, 176 mmol). The mixture was vigorously stirred for 4 h. The organic phase was washed with H_2O and dried with $MgSO_4$, and the solvents were removed under vacuum. The residue was subjected to a neutral

Received: September 20, 2011
Published: December 30, 2011

   dx.doi.org/10.1021/ic202045a | *Inorg. Chem.* 2012, 51, 978–984

alumina chromatography (CH_2Cl_2 as the eluent) to yield a pure dark red powder of **L**. Slow evaporation of a CH_2Cl_2/MeCN (mixture 1:1 in volume) containing **L** gave single crystals after 2 days. Yield: 140 mg (32%). IR (KBr): ν 2955, 2922, 2853, 1756, 1713, 1592, 1440, 1339, 1272, 1235, 1162, 1121, 777, 723, 695, 639, 540 cm^{-1}. ^1H NMR (200.13 MHz, $CDCl_3$): δ 8.19 (s, 2H), 7.10 (s, 1H), 6.35 (s, 2H), 4.02 (s, 6H). Anal. Calcd (%) for $C_{15}H_{11}N_1O_4S_4$: C, 45.34; H, 2.77; N, 3.53. Found: C, 45.19; H, 2.93; N, 3.49.

*[Er(hfac)$_3$(**L**)]$_2$ (**1**).* $Er(hfac)_3{\cdot}2H_2O$ (16.5 mg, 0.02 mmol) was dissolved in 2.5 mL of CH_2Cl_2, and then a solution of 2.5 mL of CH_2Cl_2 containing **L** (8 mg, 0.02 mmol) was slowly added. After the solution had been stirred for 15 min, 15 mL of *n*-hexane was layered in a close flask. After 1 week at −20 °C, dark purple needles suitable for X-ray diffraction formed. Yield: 10.2 mg (43%). IR (KBr): ν 2951, 2923, 2855, 1712, 1654, 1600, 1558, 1531, 1504, 1326, 1257, 1202, 1145, 799, 661, 587 cm^{-1}. Anal. Calcd (%) for $C_{30}H_{14}Er_1F_{18}N_1O_{10}S_4$: C, 30.37; H, 1.18; N, 1.18. Found: C, 30.41; H, 1.29; N, 1.12.

Crystallography. Single crystals were mounted on a Nonius four-circle diffractometer equipped with a CCD camera and a graphite-monochromated Mo Kα radiation source (λ = 0.71073 Å), from the Centre de Diffractométrie (CDFIX, Université de Rennes 1). Data were collected at 293 K. Structures were determined with a direct method using SIR-97 and refined with a full matrix least-squares method on F^2 using SHELXL-97.[10] Complete crystal structure results as a CIF file, including bond lengths, angles, and atomic coordinates, are deposited as Supporting Information.

Physical Measurements. All the physical measurements for **L** and **1** were taken on dissolved single crystals. Cyclic voltametry was conducted in a CH_2Cl_2 solution, containing 0.1 M $N(C_4H_9)_4PF_6$ as the supporting electrolyte. Voltammograms were recorded at 100 mV/s at a platinum disk electrode. The potentials were measured versus a saturated calomel electrode (SCE). Optical spectra were measured using the KBr disk method on a Perkin-Elmer 1600 Series FT-IR instrument (4 cm^{-1} resolution) for the infrared (IR) range and on a Varian Cary 5000 UV−visible−NIR spectrometer. The luminescence spectra were recorded using a Horiba-JobinYvon Fluorolog-3 spectrofluorimeter, equipped with a three-slit double-grating excitation and emission monochromator with dispersions of 2.1 nm/mm (1200 grooves/mm). The steady state luminescence was excited by unpolarized light from a 450 W xenon continuous wave lamp and detected at an angle of 90° for diluted solution measurements or 22.5° for solid state measurements (front face detection) by a Peltier-cooled red-sensitive Hamamatsu R2658P photomultiplier tube (300−1010 nm). Spectra were reference corrected for both the excitation source light intensity variation (lamp and grating) and the emission spectral response (detector and grating). Uncorrected near-infrared spectra were recorded at an angle of 45° using a liquid nitrogen-cooled, solid indium/gallium/arsenic detector (850−1600 nm). ^1H NMR spectra were recorded at room temperature on a BRUKER AC 200 MHz instrument operating at 200.13 MHz. Data are listed in parts per million and are reported relative to tetramethylsilane; residual solvent peaks of the deuterated solvents were used as an internal standard. The powder measurements of the **L** and **1** compounds were taken using scanning electron microscopy. All observations and measurements were made with a JEOL JSM 6400 scanning electron microscope (JEOL Ltd., Tokyo, Japan) with an EDS analysis system (OXFORD Link INCA). The voltage was kept at 9 kV, and the samples were mounted on carbon stubs and coated for 5 min with a gold/palladium alloy using a sputter coater (Jeol JFC 1100). This analysis was performed by the Centre de Microscopie Electronique à Balayage et microAnalyse (CMEBA) at the Université de Rennes 1.

The dc magnetic susceptibility measurements were performed on a solid polycrystalline sample with a Cryogenic S600 SQUID magnetometer between 2 and 300 K under a magnetic field of 100 Oe for temperatures of 2−65 K, 1 kOe for temperatures of 65−250 K, and 10 kOe for temperatures of 250−300 K. These measurements were all corrected for the diamagnetic contribution as calculated with Pascal's constants. All measurements were performed on pellets to prevent orientation on these very anisotropic materials.

Computational Details. The UV−visible absorption spectrum of ligand **L** was calculated. At first, a C_s symmetry geometry optimization of **L** was conducted using density functional theory (DFT) methods starting from the solid state geometry. All calculations were performed with the hybrid functional adaptation of PBE[11] (usually termed PBE0) as implemented in Gaussian09.[12] To manage the calculation on **L**, we used a triple-ζ quality basis set proposed by Weigend et al. with polarization functions for all atoms (TZVPP).[13] All the details for the polarization functions included in the triple-ζ quality basis are given in the Supporting Information. Then, the monoelectronic excitations were computed using TD-DFT procedure with the same program, functional, and basis set that were used in the first step.

RESULTS AND DISCUSSION

Synthesis. The ligand **L** is synthesized by the Stille palladium-catalyzed cross coupling [using $Pd(PPh_3)_4$] between the tributylstannyl-tetrathiafulvalene[8] and the 4-iodo-2,6-pyridinedicarboxylic acid dimethyl ester[9] in refluxing dry toluene. Equimolar reaction between **L** and the $Er(hfac)_3{\cdot}2H_2O$ precursor in CH_2Cl_2 leads to the formation of the desired complex **1** in 43% yield after crystallization. The ligand was characterized by ^1H NMR, whereas the paramagnetic complex presents only broad signals that could not be assigned. Complexation was evidenced by FTIR spectroscopy showing the expected low-energy shift of the ν(C═O) vibration of the ester moieties upon complexation[6] (from 1756 cm^{-1} in **L** to 1712 cm^{-1} in **1**). Finally, both the ligand and the complex give nice single crystals suitable for X-ray diffraction analysis.

X-ray Structural Studies. *4-Tetrathiafulvalene-2,6-pyridinedicarboxylic Acid Dimethyl Ester (**L**).* **L** crystallizes in the orthorhombic $P2_12_12_1$ space group (Table 1). The ORTEP view shows the asymmetric unit (Figure 1). The structure reveals that both the TTF core and the 2,6-pyridinedicarboxylic acid dimethyl ester are planar. The C3═C4 distance [1.351(5) Å] confirms the neutral form of **L**. The crystal packing shows the formation of columns along the *a* axis (Figure S1 of the Supporting Information) through $\pi-\pi$ interactions and S2···S4

Table 1. X-ray Crystallographic Data for L and 1

	L	1
formula	$C_{15}H_{11}NO_4S_4$	$C_{60}H_{28}N_2O_{20}S_8F_{36}Er_2$
M (g/mol)	397.5	2371.8
crystal system	orthorhombic	hexagonal
space group	$P2_12_12_1$ (No. 19)	$P3_1$ (No. 159)
unit cell parameters	a = 5.560(5) Å	a = 17.910(5) Å
	b = 9.074(4) Å	b = 17.910(5) Å
	c = 33.529(14) Å	c = 22.424(5) Å
	$\alpha = \beta = \gamma = 90°$	$\alpha = \beta = 90°$
		$\gamma = 120°$
volume (Å^3)	1691.6(18)	6229(3)
cell formula units	Z = 4	Z = 3
T (K)	293(2)	293(2)
diffraction reflection	$2.42° \le 2\theta \le 54.94°$	$2.62° \le 2\theta \le 51.36°$
ρ_{calc} (g/cm^3)	1.561	1.897
μ (mm^{-1})	0.581	2.355
no. of reflections	26278	23555
no. of independent reflections	3867	15705
$I > 2\sigma(I)$	2919	9857
no. of variables	217	1290
R_{int}, R_1, wR_2	0.0534, 0.0418, 0.0951	0.0349, 0.0661, 0.1577

dx.doi.org/10.1021/ic202045a | Inorg. Chem. 2012, 51, 978−984

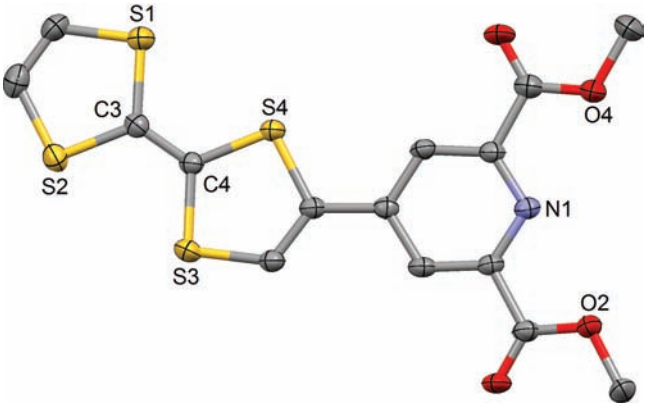

Figure 1. ORTEP view of 4-tetrathiafulvalene-2,6-pyridinedicarboxylic acid dimethyl ester **L**. Thermal ellipsoids are drawn at a 30% probability level. Hydrogen atoms have been omitted for the sake of clarity.

contacts [3.740(10) Å]. The cohesion of the crystal takes place thanks to S1···O3 [3.215(6) Å] contacts and hydrogen bonds [O1···H5, 2.394(5) Å] (Figure S1 of the Supporting Information).

*[Er(hfac)$_3$(**L**)]$_2$ (**1**).* **1** crystallizes in the hexagonal $P3_1$ space group (Table 1). The asymmetric unit includes two crystallographically independent [Er(hfac)$_3$(**L**)] molecules (Figure 2). Each molecule is composed of one Er(III) ion, three bis-chelate hfac$^-$ anions, and one **L** acting as a tris-chelating ligand. **L** ligands are coordinated to the Er(III) ions through the oxygen atoms of the carbonyl groups (O1 and O3 for Er1 and O11 and O13 for Er2) and the nitrogen atoms of the pyridine rings (N1 for Er1 and N2 for Er2) (Figure 2). Six additional oxygen atoms from three hfac$^-$ ligands complete the coordination sphere of each Er(III) ion. The erbium surroundings can be described as distorted 4,4,4-tricapped trigonal prisms. The coordination polyhedra have a D_{3h} symmetry. The Er−O and Er−N distances range from 2.300(13) to 2.508(14) Å and from 2.500(15) to 2.512(13) Å, respectively. The **L** ligands remain almost planar after the coordination of the Er(hfac)$_3$ moiety, and the mean C═C central bond [1.345(20) Å] attests to the neutrality of **L** in **1**. Both [Er(hfac)$_3$(**L**)] molecules of the asymmetric unit are stacked in a "head-to-tail" fashion because of to the $\pi-\pi$ interactions between the pyridine rings and the TTF cores (Figure 2). The crystal packing reveals a one-dimensional organic network formed by the **L** donors along the *c* axis (Figure 3). The latter is encapsulated in the inorganic network formed by the Er(hfac)$_3$ moieties (Figure 3).

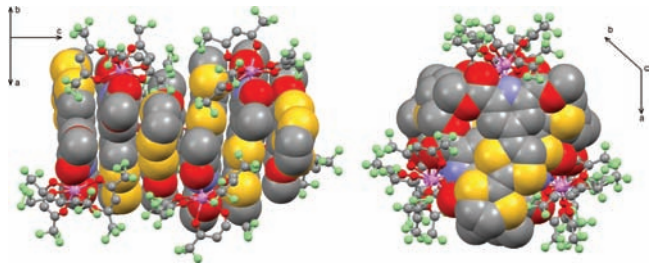

Figure 3. Crystal packing of **1** highlighting the one-dimensional organic network (space filling) along the *c* axis and its encapsulation in the inorganic one (balls and sticks).

Electrochemical Properties. The electrochemical properties of **L** and **1** have been studied by cyclic voltammetry (Figure S2 of the Supporting Information). For both compounds, two reversible single-electron-oxidation waves are observed at 490 and 890 mV (for **L**) and 480 and 880 mV (for **1**) versus SCE, corresponding successively to the formation of the radical cations and dicationic species, respectively. These values are anodically shifted in comparison with the oxidation potentials measured for the parent TTF (380 and 770 mV, respectively) due to the electron-withdrawing nature of the 2,6-pyridinedicarboxylic acid dimethyl ester substituent, which makes oxidation of the TTF core more difficult for free ligand **L** and in coordination complex **1**. It is quite surprising that no significant shift of the oxidation potentials is observed between **L** and **1**, signifying that the electronic communication between the TTF core and the Er(III) center is very weak.

Static Magnetic Properties. The thermal dependence of the $\chi_M T$ product and first magnetization for **1** are shown in Figure S3 of the Supporting Information. The room-temperature value of $\chi_M T$ is equal to 22.10 cm^3 K mol^{-1} (compared to the theoretical value of 22.96 cm^3 K mol^{-1}),[14] while it is equal to 10.99 cm^3 K mol^{-1} at 2 K for two Er(III) ions. The 4f^{11}electronic configuration is split into $^{2S+1}$L spectroscopic

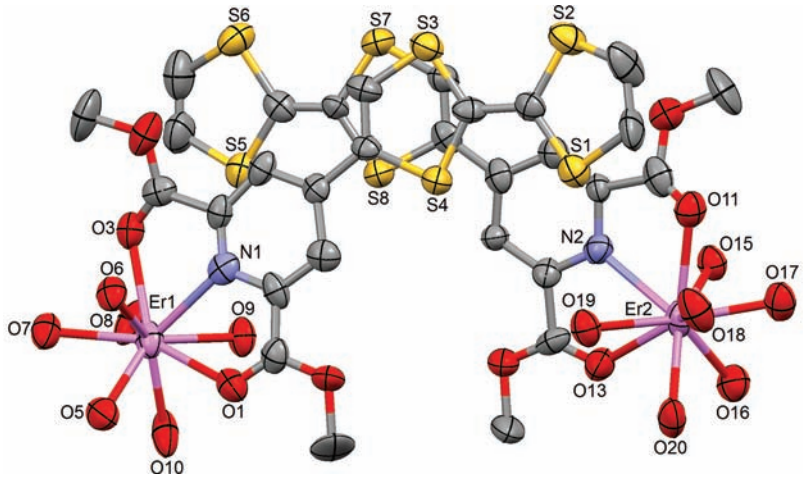

Figure 2. Simplified ORTEP view of the asymmetric unit of **1** (30% probability ellipsoids). Hydrogen atoms have been omitted for the sake of clarity.

dx.doi.org/10.1021/ic202045a | *Inorg. Chem.* 2012, 51, 978−984

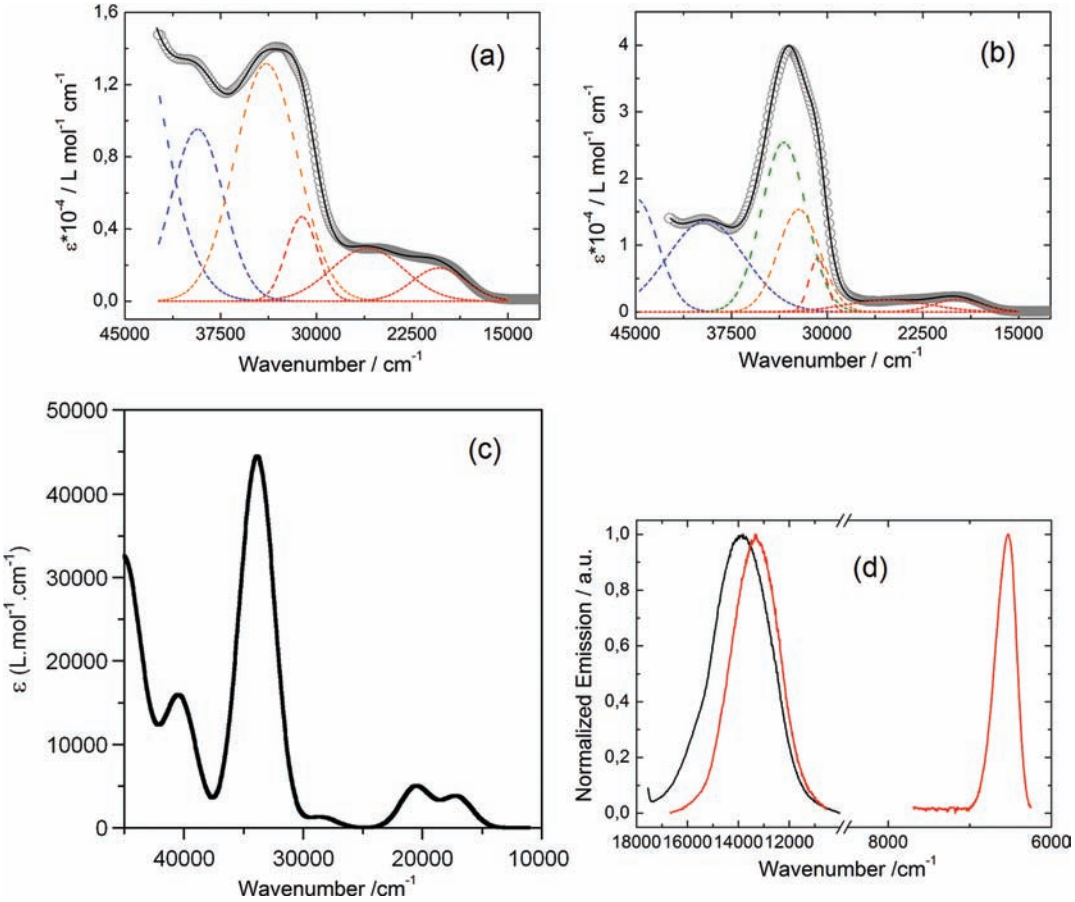

Figure 4. Experimental $CHCl_3$ solution UV−visible absorption spectra ($C = 4 \times 10^{-5}$ M) for **L** (left) and **1** (right) (gray spheres). Gaussian deconvolutions are shown as dashed lines and the best fits as solid black lines ($R = 0.9997$ and 0.9995 for **L** and **1**, respectively). (c) Theoretical absorption spectrum of the C_s symmetry structure of **L** (half-bandwidths set to 3000 cm^{-1}). (d) Room-temperature emission spectra of **L** (black) and **1** (red) in a CH_2Cl_2 solution.

terms by interelectronic repulsions, and the highest spin multiplicity term (^4I) is the lowest in energy. Each ^{2S+1}L term is split into $^{2S+1}L_J$ spectroscopic levels by spin−orbit coupling where $|L - S| \leq J \leq L + S$. The ground state of Nd(III) is then $^4I_{15/2}$ with a Zeeman factor $g_{15/2}$ equal to $^6/_5$.[15] Finally, each $^{2S+1}L_J$ term is split by crystal field in Stark sublevels separated by ~100 cm^{-1}.[16] This splitting is smaller than for first transition metallic ions because the 4f orbitals are not involved in the first approximation in the bonds with neighboring atoms. In addition, the energy splitting between the ground state $^4I_{15/2}$ and the first exited state $^4I_{13/2}$ is equal to 6540 cm^{-1} (this value is determined from the emission spectrum of **1**). Therefore, at room temperature, only the Stark sublevels from the $^4I_{15/2}$ ground state are populated. When the temperature decreases, the depopulation of these sublevels leads to a deviation from the Curie law observed by a variation of the $\chi_M T$ product even in the absence of any exchange interaction. The room-temperature value of $\chi_M T$ is in agreement with the expected value for one isolated Er(III) ion in a ErO8N1 crystal field, and the decrease in the $\chi_M T$ product can be attributed to the crystal field effect.

Photophysical Properties. The optical properties of **L** and **1** have been studied by UV−visible absorption spectroscopy in a $CHCl_3$ solution. Rationalization by TD-DFT[17] calculations was performed for **L** (Figure 4). The molecular orbital diagram and UV−visible absorption spectra were determined for **L** considering a C_s symmetry (Figures 4 and 5, Table 2, and Tables S1 and S2 of the Supporting Information).

The experimental absorption curve of **L** has been deconvoluted into six bands (Figure 4a and Table 2). The calculated UV−visible absorption spectrum for **L** in C_s symmetry reproduces the experimental **L** curve well (Figure 4c). The two lowest-energy bands have been calculated to be 17116 and 20585 cm^{-1} (red deconvolutions localized at 20400 and 26000 cm^{-1}, respectively), and they have been attributed to $\pi-\pi^*$ HOMO → LUMO (98%) and HOMO → LUMO + 1 (99%) donor to acceptor charge transfers (DACTs), respectively (Table 2).[3] The absorption band centered at 31100 cm^{-1} (red deconvolution) has been calculated to be at 33399 cm^{-1} and attributed to the $\pi-\pi^*$ HOMO − 1 → LUMO (81%) DACT (Table 2). The absorption band centered at 33900 cm^{-1} (orange deconvolution) has been calculated to be at 34676 cm^{-1} and has been attributed to the $\pi-\pi^*$ HOMO → LUMO + 5 (72%) intradonor transition (Table 2). The next absorption band at 39300 cm^{-1} (blue deconvolution) corresponds to both excitations calculated to be at 40050 and 41260 cm^{-1}, corresponding to the $\pi-\pi^*$ HOMO − 3 and HOMO − 4 → LUMO intra-acceptor (IA) transitions, respectively (Table 2). Finally, the highest-energy Gaussian deconvolution is centered at 45500 cm^{-1}, which corresponds to the $\pi-\pi^*$ absorption bands calculated to be at 44339 and 45863 cm^{-1} and identified as a combination of IA (HOMO − 3 → LUMO + 1 and HOMO − 4 → LUMO + 1) and DACT (HOMO − 6 → LUMO)

dx.doi.org/10.1021/ic202045a | Inorg. Chem. 2012, 51, 978−984

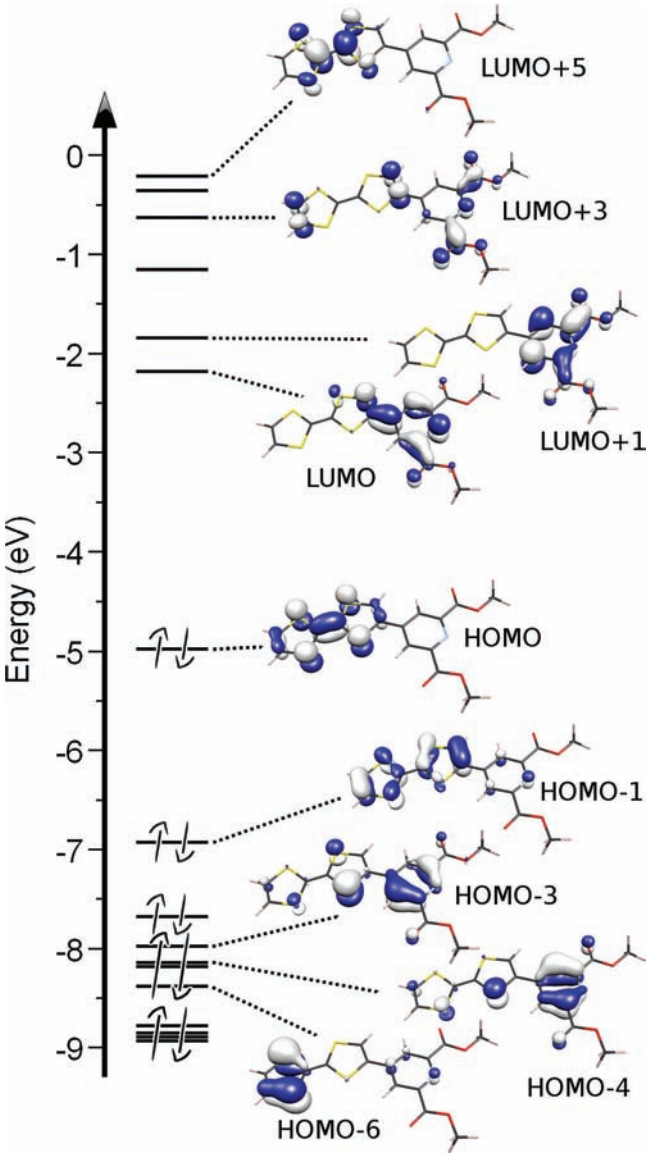

Figure 5. Molecular orbital diagram of the C_s symmetry structure of **L**. Contour values are ±0.05 $(e^-/Bohr^3)^{1/2}$.

excitations. It is worth noting that a DACT contribution is identified for almost all the absorption bands (Table 2). The strong donor and acceptor characters of the TTF core and the 2,6-pyridinedicarboxylic acid dimethyl ester substituent explain these DACT contributions.

The absorption spectrum of **1** has been deconvoluted into seven bands that are localized at the following energies: 19800, 25200, 30700, 32200, 33400, 39500, and 45000 cm^{-1} (Figure 4b). It shows a new intense absorption excitation centered at 33400 cm^{-1} that corresponds to $\pi-\pi^*$ intra-hfac$^-$ excitations.[3] As expected, complexation induces a marked red shift of the ligand-centered DACT transition due to the Lewis acid behavior of the Er(III) metal center enforcing the electron-withdrawing character of the 2,6-pyridinedicarboxylic acid dimethyl ester fragment.[3] Thus, the absorption bands are red-shifted from 500 to 1000 cm^{-1} in **1** compared to those in **L** due to the DACT contributions. The pure IA band remains at the same energy (39500 cm^{-1}). The emission properties were measured at room temperature in a freshly distilled dichloromethane solution. For complex **1**, the measurements were performed in the 10^{-3}–10^{-4} mol/L concentration range because dissociation occurs at higher dilutions. Excitation in the ligand (**L**) DACT (λ_{ex} = 18–20000 cm^{-1}) results in the observation of a broad emission band centered at 13900 cm^{-1} [720 nm (Figure 4d)], characteristic of TTF-containing ligands.[3,18] Upon similar excitation in the lowest-energy transition of complex **1**, two emissions are observed: a ligand-centered one at 13300 cm^{-1} (750 nm) exhibiting the same red shift observed in absorption and a second emission in the NIR at 6540 cm^{-1} (1530 nm) characteristic of the Er(III) $^4I_{13/2} \rightarrow {}^4I_{15/2}$ transition. Similar photophysical properties were obtained in the solid state (Figure 6 and Figure S4 of the Supporting Information).

The energy of the donor excited state can be evaluated from the zero-phonon transition wavenumber and estimated to be ~16600 cm^{-1} (602 nm) from the intersection of the absorption and emission spectra. The presence of the low-energy DACT transition strongly suggests that the sensitization occurs directly via the transfer of energy from the charge transfer state without participation of the triplet excited state.[3] Such a direct sensitization process is well-documented for Eu(III) and also for Nd and Yb(III) ions[7b,19] but is more scarce for Er(III)[20] and

Table 2. Energies Calculated via TD-DFT, Assignments, and Major Contributions in the Transitions of the Most Pertinent Low-Lying Electronic Excitations of the C_s Symmetry Structure of L[a]

exptl energy (cm^{-1})	calcd energy (cm^{-1})	oscillation	type	%D	%A	assignment	transition
20400	17116	0.05	DACT	97 → 31	3 → 69	$\pi_D \rightarrow \pi^*_A$	H → L (98%)
26000	20585	0.07	DACT	97 → 2	3 → 98	$\pi_D \rightarrow \pi^*_A$	H → L + 1 (99%)
31100	33399	0.40	DACT (+ID)	89 → 41	11 → 59	$\pi_D \rightarrow \pi^*_A$ ($\pi_D \rightarrow \pi^*_D$)	H − 1 → L (81%), H → L + 5 (15%)
33900	34676	0.28	ID (+DACT)	95 → 76	5 → 24	$\pi_D \rightarrow \pi^*_D$ ($\pi_D \rightarrow \pi^*_A$)	H → L + 5 (72%), H − 1 → L + 1 (14%), H → L (10%)
39300	40050	0.15	IA (+DACT)	51 → 23	49 → 77	$\pi_A \rightarrow \pi^*_A$ ($\pi_D \rightarrow \pi^*_A$)	H − 3 → L (63%), H − 1 → L + 1 (13%), H − 4 → L (8%)
	41260	0.09	IA	38 → 27	62 → 73	$\pi_A \rightarrow \pi^*_A$	H − 4 → L (61%), H − 3 → L (19%), H − 3 → L + 1 (12%)
45500	44339	0.23	IA DACT	60 → 20	40 → 80	$\pi_A \rightarrow \pi^*_A$ ($\pi_D \rightarrow \pi^*_L$)	H − 3 → L + 1 (46%), H − 1 → L + 3 (22%), H − 6 → L (10%), H − 4 → L + 1 (9%)
	45863	0.19	DACT IA	74 → 30	26 → 70	$\pi_D \rightarrow \pi^*_A$, $\pi_A \rightarrow \pi^*_A$	H − 6 → L (35%), H − 4 → L + 1 (21%), H → L + 9 (14%)

[a]D, A, H, and L represent TTF (donor), 2,6-pyridinedicarboxylic acid dimethyl ester (acceptor), the HOMO, and the LUMO, respectively; therefore DACT stands for donor to acceptor charge transfer, ID for intradonor, and IA for intra-acceptor.

dx.doi.org/10.1021/ic202045a | Inorg. Chem. 2012, 51, 978–984

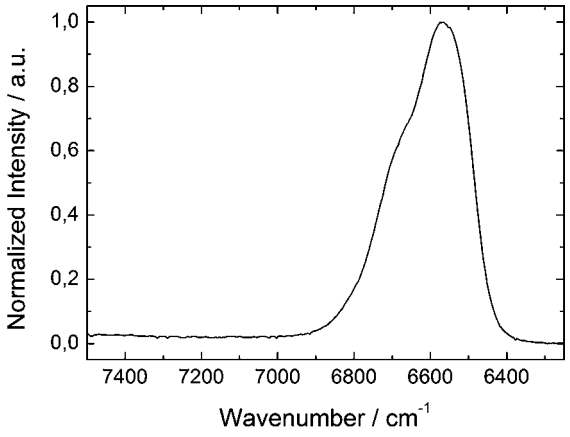

Figure 6. Solid state emission of **1** in the NIR spectral range.

to the best of our knowledge has never been achieved with such a low-energy antenna donating state (16600 cm^{-1}).

CONCLUSIONS

In conclusion, the synthesis and determination of the X-ray structure of a new TTF-containing ligand **L** have been performed, leading to the formation of a mononuclear $[Er(hfac)_3(\mathbf{L})]$ complex that is soluble and stable in chlorinated solvents. The strong coordination of Er(III) to the tridentate 2,6-pyridinedicarboxylic acid dimethyl ester fragment allows solution measurements (cyclic voltametry and optical properties) in concentrated chlorinated solvents, but the stability of the complex in solution remains rather modest. Electrochemistry demonstrates the redox activity of **L** and **1**, while the photophysical properties clearly indicate that TTF-based ligands are very versatile antenna chromophores, allowing not only Yb(III) and Nd(III)[3,4] but also Er(III) sensitization in solution and in the solid state. TD-DFT calculations suggest that the lowest-energy excited state is a DACT state, indicating that the sensitization occurs directly from this charge transfer state. Further optimization of this ligand family is underway to further increase both the sensitization efficiency and the solution stability. Finally, the stability of **1** in solution is an encouraging result with respect to its electrocrystallization for the preparation of a multifunctional material combining conductivity, magnetic, and luminescence properties.

ASSOCIATED CONTENT

Supporting Information

Computational details, crystallographic information in CIF format, cyclic voltammetry for **L** and **1**, and crystal packing of **L**; $\chi_M T(T)$ and $M(H)$ curves for **1**; and solid state luminescence spectra for **L**. This material is available free of charge via the Internet at http://pubs.acs.org.

AUTHOR INFORMATION

Corresponding Author

*E-mail: Lahcène.ouahab@univ-rennes1.fr.

ACKNOWLEDGMENTS

This work was supported by the CNRS, Rennes Métropole, Université de Rennes 1, Région Bretagne, and FEDER.

REFERENCES

(1) (a) Kobayashi, A.; Fijiwara, E.; Kobayashi, H. *Chem. Rev.* **2004**, *104*, 5243. (b) Enoki, T.; Miyasaki, A. *Chem. Rev.* **2004**, *104*, 5449. (c) Coronado, E.; Day, P. *Chem. Rev.* **2004**, *104*, 5419. (d) Ouahab, L.; Enoki, T. *Eur. J. Inorg. Chem.* **2004**, 933.

(2) (a) Lorcy, D.; Bellec, N.; Fourmigué, M.; Avarvari, N. *Coord. Chem. Rev.* **2009**, *253*, 1398. (b) Setifi, F.; Ouahab, L.; Golhen, S.; Yoshida, Y.; Saito, G. *Inorg. Chem.* **2003**, *42*, 1791.

(3) (a) Pointillart, F.; Maury, O.; Le Gal, Y.; Golhen, S.; Cador, O.; Ouahab, L. *Inorg. Chem.* **2009**, *48*, 7421. (b) Pointillart, F.; Cauchy, T.; Maury, O.; Le Gal, Y.; Golhen, S.; Cador, O.; Ouahab, L. *Chem.—Eur. J.* **2010**, *16*, 11926.

(4) (a) Faulkner, S.; Burton-Pye, B. P.; Khan, T.; Martin, L. R.; Wray, S. D.; Skabara, P. J. *Chem. Commun.* **2002**, *16*, 1668. (b) Pope, S. J. A.; Burton-Pye, B. P.; Berridge, R.; Khan, T.; Skabara, P.; Faulkner, S. *Dalton Trans.* **2006**, 2907.

(5) Lazarides, T.; Alamiry, M. A. H.; Adams, H.; Pope, S. J. A.; Faulkner, S.; Weinstein, J. A.; Ward, M. D. *Dalton Trans.* **2007**, 1484.

(6) (a) Renaud, F.; Piguet, C.; Bernardinelly, G.; Bünzli, J. C. G.; Hopfgartner, G. *Chem.—Eur. J.* **1997**, *3*, 1646. (b) Renaud, F.; Piguet, C.; Bernardinelly, G.; Bünzli, J. C. G.; Hopfgartner, G. *Chem.—Eur. J.* **1997**, *3*, 1660. (c) Muller, G.; Schmidt, B.; Hopfgartner, G.; Riehl, J. P.; Bünzli, J. C. G.; Piguet, C. *J. Chem. Soc., Dalton Trans.* **2001**, 2655.

(7) (a) Picot, A.; Malvolti, F.; Le Guennic, B.; Baldeck, P. L.; Williams, J. A. G.; Andraud, C.; Maury, O. *Inorg. Chem.* **2007**, *46*, 2659. (b) D'Aléo, A.; Picot, A.; Beeby, A.; Williams, J. A. G.; Le Guennic, B.; Andraud, C.; Maury, O. *Inorg. Chem.* **2008**, *47*, 10258.

(8) Bouguessa, S.; Gouasmia, A. K.; Golhen, S.; Ouahab, L.; Fabre, J. M. *Tetrahedron Lett.* **2003**, *44*, 9275.

(9) Picot, A.; Feuvrie, C.; Barsu, C.; Malvolti, F.; Le Guennic, B.; Le Bozec, H.; Andraud, C.; Toupet, L.; Maury, O. *Tetrahedron* **2008**, *64*, 399.

(10) (a) Otwinowski, Z.; Minor, W. Processing of X-ray Diffraction Data Collected in Oscillation Mode. In *Methods in Enzymology, Volume 276: Macromolecular Crystallography, Part A*; Carter, C. W., Sweet, R. M., Jr., Eds.; Academic Press: San Diego, **1997**; pp 307−326.

(11) (a) Perdew, J. P.; Burke, K.; Ernzerhof, M. *Phys. Rev. Lett.* **1996**, *77*, 3865. (b) Adamo, C.; Barone, V. *J. Chem. Phys.* **1999**, *110*, 6158.

(12) Frisch, M. J.; Trucks, G. W.; Schlegel, H. B.; Scuseria, G. E.; Robb, M. A.; Cheeseman, J. R.; Scalmani, G.; Barone, V.; Mennucci, B.; Petersson, G. A.; Nakatsuji, H.; Caricato, M.; Li, X.; Hratchian, H. P.; Izmaylov, A. F.; Bloino, J.; Zheng, G.; Sonnenberg, J. L.; Hada, M.; Ehara, M.; Toyota, K.; Fukuda, R.; Hasegawa, J.; Ishida, M.; Nakajima, T.; Honda, Y.; Kitao, O.; Nakai, H.; Vreven, T.; Montgomery, J. A., Jr.; Peralta, J. E.; Ogliaro, F.; Bearpark, M.; Heyd, J. J.; Brothers, E.; Kudin, K. N.; Staroverov, V. N.; Kobayashi, R.; Normand, J.; Raghavachari, K.; Rendell, A.; Burant, J. C.; Iyengar, S. S.; Tomasi, J.; Cossi, M.; Rega, N.; Millam, J. M.; Klene, M.; Knox, J. E.; Cross, J. B.; Bakken, V.; Adamo, C.; Jaramillo, J.; Gomperts, R.; Stratmann, R. E.; Yazyev, O.; Austin, A. J.; Cammi, R.; Pomelli, C.; Ochterski, J. W.; Martin, R. L.; Morokuma, K.; Zakrzewski, V. G.; Voth, G. A.; Salvador, P.; Dannenberg, J. J.; Dapprich, S.; Daniels, A. D.; Farkas, Ö.; Foresman, J. B.; Ortiz, J. V.; Cioslowski, J.; Fox, D. J. *Gaussian09*, revision A.02; Gaussian, Inc.: Wallingford, CT, 2009.

(13) Weigend, F.; Ahlrichs, R. *Phys. Chem. Chem. Phys.* **2005**, *7*, 3297.

(14) Kahn, O. *Molecular Magnetism*; VCH: Weinheim, Germany, 1993.

(15) Benelli, C.; Gatteschi, D. *Chem. Rev.* **2002**, *102*, 2369.

(16) Sutter, J.-P.; Kahn, M. L. *Magnetism: Molecules to materials V*; VCH: Weinheim, Germany, 2005.

(17) De Silva, C. R.; Li, J.; Zheng, Z.; Corrales, L. R. *J. Phys. Chem. A* **2008**, *112*, 4527.

(18) Jia, C.; Liu, S.-X.; Tanner, C.; Leiggener, C.; Neels, A.; Sanguinet, L.; Levillain, E.; Leutwyler, S.; Hauser, A.; Decurtins, S. *Chem.—Eur. J.* **2007**, *13*, 3804.

(19) (a) Eliseeva, S. V.; Bünzli, J.-C. G. *Coord. Soc. Rev.* **2010**, *39*, 189. (b) Andraud, C.; Maury, O. *Eur. J. Inorg. Chem.* **2009**, 4357. (c) Huang, W.; Wu, D.; Guo, D.; Zhu, X.; He, C.; Meng, Q.; Duan, C. *Dalton Trans.* **2009**, 2081. (d) Yang, C.; Fu, L.-M.; Wang, Y.; Zhang, J.-P.;

Wong, W.-T.; Ai, X.-C.; Qiao, Y.-F.; Zou, B.-S.; Gui, L.-L. *Angew. Chem., Int. Ed.* **2004**, *43*, 5010. (e) Hebbink, G. A.; Klink, S. I.; Grave, L.; Oude Alink, P. G. B.; van Veggel, F. C. J. M. *ChemPhysChem* **2002**, *3*, 1014. (f) Ziessel, R. F.; Ulrich, G.; Charbonnière, L.; Imbert, D.; Scopelliti, R.; Bünzli, J.-C. G. *Chem.—Eur. J.* **2006**, *12*, 5060. (g) Shavaleev, N. M.; Scopelliti, R.; Gumy, F.; Bünzli, J.-C. G. *Inorg. Chem.* **2009**, *48*, 2908.

(20) (a) Werts, M. H. V.; Hofstraat, J. W.; Geurts, F. A. J.; Verhoeven, J. W. *Chem. Phys. Lett.* **1997**, *276*, 196. (b) Shavaleev, N. M.; Scopelliti, R.; Gumy, F.; Bünzli, J.-C. G. *Eur. J. Inorg. Chem.* **2008**, 1523. (c) Baek, N. S.; Kim, Y. H.; Eom, Y. K.; Oh, J. H.; Kim, H. K.; Aebischer, A.; Gumy, F.; Chauvin, A.-S.; Bünzli, J.-C. G. *Dalton Trans.* **2010**, *39*, 1532. (d) Albrecht, M.; Osetska, O.; Klankermayer, J.; Fröhlich, R.; Gumy, F.; Bünzli, J.-C. G. *Chem. Commun.* **2007**, 1834.